Optimization of sequential therapies to maximize extinction of resistant bacteria through collateral sensitivity

Javier Molina-Hernández [1,2] José A. Cuesta [1,2,3] Beatriz Pascual-Escudero [4] Saúl Ares [2,5,*] and Pablo Catalán [1,2,†]

[1] *Universidad Carlos III de Madrid, Departamento de Matemáticas, Leganés, Spain*

[2] *Grupo Interdisciplinar de Sistemas Complejos (GISC), 28911 Leganés, Spain*

[3] *Instituto de Biocomputación y Física de Sistemas Complejos, Universidad de Zaragoza, Zaragoza, Spain*

[4] *Universidad Politécnica de Madrid, Madrid, Spain*

[5] *Centro Nacional de Biotecnologia (CNB), CSIC, Madrid, Spain*

(Received 4 November 2025; accepted 24 March 2026; published 8 May 2026)

Antimicrobial resistance (AMR) threatens global health. A promising and underexplored strategy to tackle this problem is sequential therapies exploiting collateral sensitivity (CS), whereby resistance to one drug increases sensitivity to another. Here, we develop a four-genotype stochastic birth-death model with two bacteriostatic antibiotics to identify switching periods that maximize bacterial extinction under subinhibitory concentrations. We show that extinction probability depends nonlinearly on switching period, with stepwise increases aligned to discrete switch events: fast sequential therapies are suboptimal as they do not allow for the evolution of resistance, a key ingredient in these therapies. A geometric distribution framework accurately predicts cumulative extinction probabilities, where the per-switch extinction probability rises with switching period. We further derive a heuristic approximation for the extinction probability based on times to fixation of single-resistant mutants. Sensitivity analyses reveal that strong reciprocal CS is required for this strategy to work, and we explore how increasing antibiotic doses and higher mutation rates modulate extinction in a nonmonotonic manner. Finally, we discuss how longer therapies maximize extinction but also cause higher resistance, leading to a Pareto front of optimal switching periods. Our results provide quantitative design principles for *in vitro* and clinical sequential antibiotic therapies, underscoring the potential of CS-guided regimens to suppress resistance evolution and eradicate infections.

DOI: 10.1103/zty8-yj5p

I. INTRODUCTION

Antimicrobial resistance (AMR) is rising rapidly [1], leading to higher rates of uncontrolled infections that contribute significantly to both patient mortality and healthcare costs [2]. The development of new antibiotics is not fast enough to counteract this problem [3] and, although new technologies can help accelerate discovery [4], this is not guaranteed to solve the problem, as resistance to new antibiotics evolves soon after or even before their deployment in the clinic [5,6].

An alternative strategy to combat AMR is to develop multidrug treatments [7], unlocking access to large combinatorial treatment spaces. Combination therapies are the most explored alternative, where two or more antibiotics are deployed simultaneously [8]. These therapies can prevent the rise of AMR [9], especially if the antibiotics are chosen *ad hoc* for a particular pathogen [10] or based on their interaction profiles [11]. However, combination therapies are not without disadvantages: the total concentration of antibiotics introduced in the patient is higher than monotherapies, and so there is the risk of toxic effects [12]. Moreover, combinations have sometimes been found to accelerate, rather than slow down, the appearance of resistance [13,14].

A less explored alternative to combination therapies is sequential therapies, in which several antibiotics are administered one after the other instead of simultaneously [15]. This strategy is based on the phenomenon of collateral sensitivity (CS), in which bacterial resistance to one antibiotic increases its sensitivity to another. CS has been found in many bacterial species and antibiotic classes [16–19], suggesting a promising avenue to develop treatments that can eradicate pathogenic bacterial populations [20,21]. The sequential framework opens the door to mathematical optimization approaches, where we seek the optimal sequence that maximizes the eradication of the population or minimizes the evolution of resistance [22–27].

Here, we seek antibiotic switching protocols that maximize bacterial extinction in a stochastic population model where only four genotypes and two antibiotics are considered, similarly to previous work [28]. While transmission dynamics between different patients are a critical element driving the AMR crisis and have been studied in depth before [29–31], we focus on within-host evolutionary dynamics, a key yet poorly understood aspect of AMR [32] where *de novo* mutations can appear in the span of days or weeks [33–36].

We show that sequential therapies based on strong CS can lead to bacterial eradication even at subinhibitory concentrations, provided that the correct switching period is used. The dependence of bacterial extinction on the switching period is explained by population composition, paving the

*Contact author: saul.ares@csic.es

†Contact author: pcatalan@math.uc3m.es

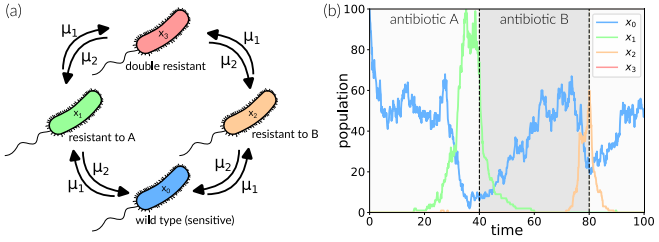

FIG. 1. Four-genotype model. (a) We consider four genotypes: x_0 (blue), susceptible to both antibiotics; x_1 (green), resistant to antibiotic A but susceptible to B; x_2 (orange), resistant to B and susceptible to A; and x_3 (red), resistant to both antibiotics. Mutation rates between the genotypes are indicated next to the corresponding arrows. (b) Illustrative trajectory. We start our simulations with antibiotic A and, after some time τ, we switch to antibiotic B, and repeat the process.

way for optimization based on population metrics. Our results are contingent on the existence of strong CS, and we observe nonmonotonic relationships between extinction rates and antibiotic dose, on one hand, and mutation rates, on the other, which we can explain using our model. We end by searching for optimal switching periods that both maximize extinction and minimize the appearance of resistance, finding there is a tradeoff between both objectives, leading to a Pareto front of optimal therapies. Our work suggests that sequential therapies are a rich opportunity to explore potentially successful strategies that will help tackle the antibiotic crisis.

II. THE MODEL

We will study bacterial population dynamics within a single patient under two bacteriostatic antibiotics A and B, using a four-genotype birth-death stochastic model. The four types are: x_0, susceptible to both antibiotics; x_1, resistant to A but susceptible to B; x_2, resistant to B but susceptible to A; and x_3, resistant to both [Fig. 1(a)]. We consider stochastic transitions (mutations) between types, with rates μ_1 for the acquisition of resistance and μ_2 for the loss of resistance [37]. Mutations from x_0 to x_3 are not permitted, although their introduction does not qualitatively change our results. We do not consider transmission of new strains from other patients, focusing instead on within-host evolutionary dynamics. In what follows, we will refer to the population of genotype x_i as N_i. Birth rates are different for each type, and depend on the antibiotic we are using. Type x_0 reproduces with rate $\beta_{0,A} = k_A\beta$ under antibiotic A and with rate $\beta_{0,B} = k_B\beta$ under antibiotic B, where $k_A, k_B \in [0, 1]$ is a measure of antibiotic inhibition: the antibiotic effect is stronger the lower the value of k. In what follows, we make the simplifying assumption $k_A = k_B = k$ and leave the analysis of other scenarios for future works. Type x_1 reproduces with birth rate $\beta_{1,A} = \beta$ under antibiotic A and with rate $\beta_{1,B} = k_{\rm CS}k_B\beta$ under antibiotic B, where $k_{\rm CS} \in [0, 1]$ is a measure of the lack of collateral sensitivity: when $k_{\rm CS} \to 1$ CS is absent, whereas when $k_{\rm CS} \to 0$ it is very strong. Birth rates for type x_2 are symmetrical to those of type x_1. Birth rates for type x_3 are $\beta_{3,A} = \beta_{3,B} = \beta$ in both antibiotics. For simplicity of notation, we will nondimensionalize time by defining the variable βt, which is equivalent to setting $\beta = 1$.

Death rates are equal for all types and antibiotics and equal to $\delta_{i,A} = \delta_{i,B} = \gamma N$, $i = 0, 1, 2, 3$, where $N = N_0 + N_1 + N_2 + N_3$ is the total population, simulating limited resources. Note that $\gamma\beta_{i,j}^{-1}$ is the inverse of the carrying capacity in logistic models. We fix $\gamma = 0.01$ (one death per one hundred births).

For computational efficiency, in order to simulate the stochastic model we will use the tau-leaping algorithm [38], which approximates the dynamics of the birth-death process by taking small time increments dt and generating pseudo-random Poisson-distributed numbers for all reactions: births, deaths, and mutations. Population sizes are updated accordingly, and the process is repeated until desired. Note that using Gillespie's algorithm [39], which simulates the model exactly, does not qualitatively change our results (see Appendix A, Fig. 8).

We start our simulations with antibiotic A and initial population $N_0 = k\gamma^{-1}$, $N_1 = N_2 = N_3 = 0$, i.e., initially there is no resistance and the population of susceptible is at the carrying capacity. After some elapsed time τ (switching period) we switch from antibiotic A to B, and continue the process. At time 2τ we switch back to A and so on [Fig. 1(b)]. We are interested in studying how this parameter τ, the period of antibiotic switching, affects the probability that the population becomes extinct at the end of treatment.

We study treatments of different τ ranging from zero to 100 time units, with a fixed treatment duration $T = 100$. In our framework, treatment duration T should be understood as corresponding to a typical antibiotic regime in a clinical context: for instance, a person taking one pill every h hours for a total of T hours, with the final dose administered at time T. However, the pharmacodynamic effects of the antibiotic are not expected to vanish instantaneously at T, since this marks the time of the last administered dose rather than the cessation of its biological activity. To account for this, we simulate an additional period under the final antibiotic (i.e., with no further switches) beyond time T, and evaluate extinction probabilities based on this extended simulation. This is particularly relevant for values of τ close to T, where the last antibiotic may have been recently applied and its impact is still unfolding.

For simulation purposes, we mark a population as extinct whenever $N < 0.05\gamma^{-1}$ [40], and our results remain qualitatively unchanged by reasonable changes in this threshold (Appendix A and Fig. 9 therein).

III. RESULTS

A. Sequential treatments with strong collateral sensitivity result in bacterial eradication even with subinhibitory antibiotic concentrations

We start our study with subinhibitory antibiotic concentrations $k_A = k_B = 0.5$, usually called the half-maximum inhibitory concentration or IC50, and consider strong CS, $k_{\rm CS} = 0.05$. This may seem like a strange place to begin, as these subinhibitory doses are usually thought to promote the evolution of resistance [41,42]. However, our simulations produce a wide range of switching periods τ that result in frequent eradication of the bacterial population. Figure 2(a)

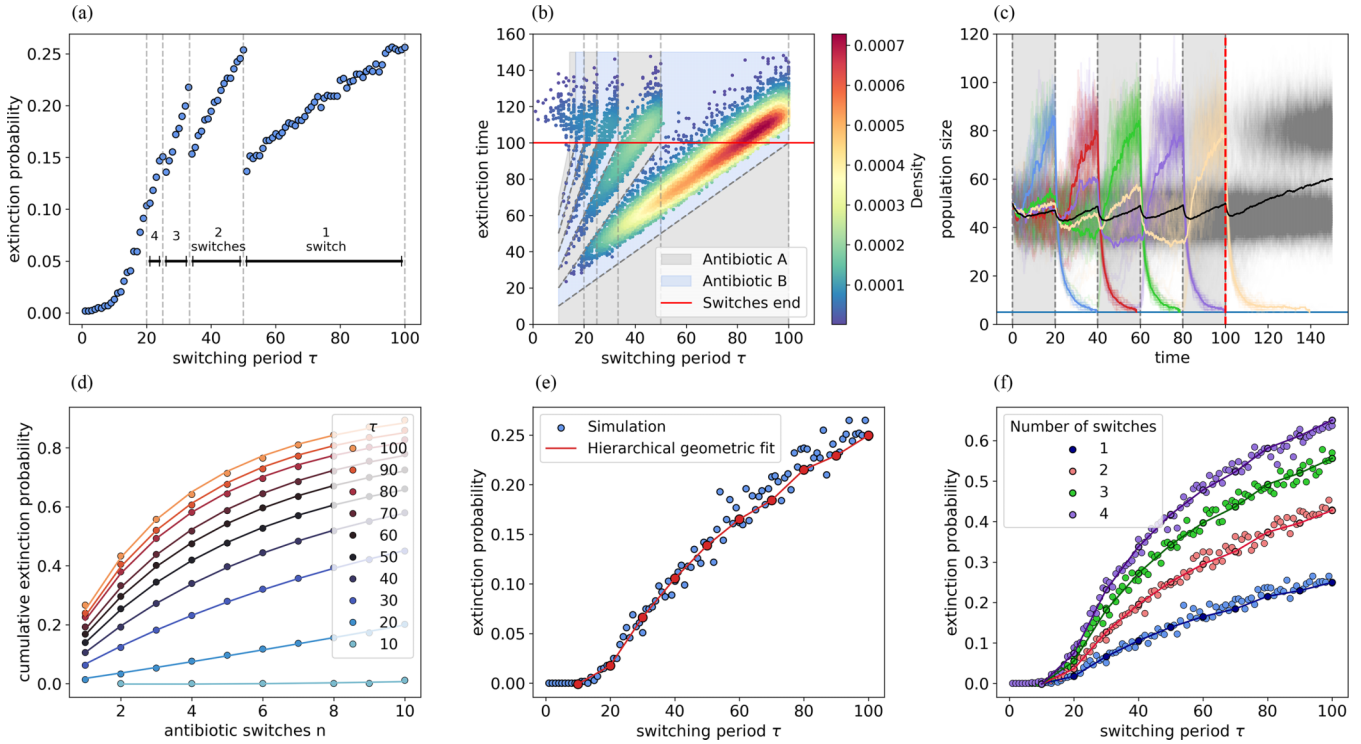

FIG. 2. Sequential therapies with subinhibitory antibiotic concentrations cause extinction for a wide range of switching periods. (a) Probability of extinction at the end of the treatment as switching periods vary. The intervals between two vertical lines share the same number of treatment cycles. 10 000 trajectories were used to estimate the probability as a function of τ. (b) Distribution of extinction times as a function of switching periods. Each point corresponds to the time a simulation became extinct. The colors represent the density of these events. The background color represents the antibiotic used. The red line represents the end of the time we allow for switching antibiotics. (c) 1000 individual trajectories switching treatment every 20 time units. Blue, red, green, purple, and orange represent the mean of trajectories that go extinct upon switching antibiotics at different switching events. Black represents the mean of those trajectories that do not become extinct. Dashed lines indicate the antibiotic switch. (d) Cumulative extinction probability over 10 treatment switches with different switching periods τ. Points represent extinction probabilities estimated through simulation, while the solid line reflects a fit to a hierarchical geometric distribution. (e) Extinction probability for populations undergoing one antibiotic switch; blue points represent the simulation, and the red points are the fitted extinction probabilities for the corresponding τ using the hierarchical geometric model (the red line is a guide to the eye). (f) Predicted extinction probabilities for populations undergoing one to four antibiotic switches using the hierarchical geometric model. Simulations were performed with final times $\tau \times$(number of switches)+50. Parameter values are in Appendix B, Table I.

shows that the probability that a population becomes extinct at the end of the treatment depends nontrivially on τ. First, we observe that there are no extinctions when $\tau \to 0$ [Figs. 2(a) and 2(b)]. As τ increases, there is a rapid increase in the probability of extinction, with two maxima at $\tau = 50$ and $\tau = 100$. The extinction probability shows some sharp discontinuities, which are due to a change in the number of antibiotic switches: extinction probabilities increase discontinuously when a new antibiotic switch is introduced. For instance, when τ is decreasing from 100, the extinction probability suddenly increases when we reach $\tau = 50$, where the number of antibiotic switches increases from 1 to 2. Similarly, when we cross the threshold $\tau = 33.3$ there is another increase in extinction probabilities, associated with an increase in the number of switches from 2 to 3. Conversely, in the absence of switches (i.e., $\tau = 0$ or $\tau > T$) there are no

TABLE I. Model parameters and their meanings.

Parameter	Description	Value
τ	Duration of treatment with antibiotic A or B	Variable
k_A, k_B	Effect of bacteriostatic antibiotics (higher ⇒ weaker inhibition)	0.5
γ	Inverse of the theoretical carrying capacity	0.01
k_{CS}	Collateral sensitivity effect (higher ⇒ weaker CS)	0.05
μ_1	Mutation rate to a resistant genotype	10^{-3}
μ_2	Mutation rate back to a sensitive genotype	10^{-2}
t_{end}	Total time of the simulation	150
$t_{\mathrm{end\ treatment}}$	Time in which we allow antibiotics to be switched	100

extinctions, which is to be expected since we are studying IC50 concentrations. Moreover, when studying extinction times, we observe that, for a fixed switching period τ, extinction events occur more frequently after a short transient period following the switching time [Fig. 2(b)] and never before the first switch. In order to better illustrate this phenomenon, we examine a collection of trajectories for fixed $\tau = 20$ [Fig. 2(c)]: some trajectories become extinct after the first switch [marked in blue in Fig. 2(c)], some after the second (red), third (green), fourth (purple), and fifth (orange) switches. Populations that do not become extinct (black) eventually gain resistance.

Since extinction events occur shortly after switching antibiotics, we can visualize the extinction process as a coin-tossing game where the probability of getting heads is p: each time the antibiotic switches, we toss a coin. If the result is heads, the population becomes extinct. The probability that the extinction event occurs exactly after n switches would then be given by the geometric probability distribution $(1-p)^{n-1}p$, where p is the probability that the population becomes extinct after one antibiotic switch, and which may be dependent on τ. The cumulative extinction probability, i.e., the probability that the population has become extinct by the nth switch, is given by $1-(1-p)^n$. The main hypothesis of this model is that p is constant throughout the process, which will be true if the time between switching is sufficiently large so that the population reaches some kind of stationary state that is independent of the switching event.

Fitting the cumulative extinction probability obtained from simulations for different τ to equation $1-(1-p)^n$ results in good agreement [Appendix C, Fig. 10(a)]. However, the fits are not perfect: they tend to underestimate the extinction probabilities when the number of switches is small, and vice versa. This suggests that p is not constant and slightly depends on the number of switches. We capture this behavior with a hierarchical geometric model where $p = \alpha\tau + \beta n$ can change with both switching period τ and the number of switches n, resulting in a great fit to the data [Fig. 2(d), Appendix C]. The values of p obtained with our fits are shown in Fig. 2(e) (red line) as a function of τ and compared with the simulated extinction probabilities for treatments undergoing only one switch (blue circles): the probability of extinction per switching event is close to zero for $\tau < 20$, consistent with what we observed in Fig. 2(a), and increases as τ grows. In other words, the longer we wait until we switch antibiotics, the higher the probability that the population becomes extinct. The agreement between the simulated per-switch extinction (blue circles) and the hierarchical geometric fit (red lines) is quite good, given the simplicity of the model. We can use this fit to predict extinction times after two or more switches, by calculating the corresponding probability using the geometric distribution, with very good agreement [Fig. 2(f)], supporting our hypothesis.

B. Heuristic explanation for the change in extinction probabilities

We turn now to give an explanation for the observed extinction patterns by finding out which variables explain the dependence of the extinction probability on the switching period τ. Figure 2(c) hints that, in those populations that become extinct, right before the switch the population had become dominated by the single-resistant populations (x_1 or x_2) reaching a carrying capacity close to 100. In contrast, the populations where extinction does not happen [marked in gray in Fig. 2(c)] are dominated by x_0, whose carrying capacity is 50. Our hypothesis is that, for small τ, resistant mutants have hardly any time to appear in the population before the antibiotic is switched and, due to the strong CS, they are rapidly invaded after the switch by type x_0, which does not go extinct under IC50 concentrations. As τ increases, however, the likelihood that either x_1 or x_2 rise in the population grows, and therefore, when the antibiotic switches, there is a chance that the whole population goes extinct.

TABLE II. Parameters in sigmoid fit of Fig. 3.

Parameter	Sigmoid fit
x_0	−0.820103
x_3	−1.243756
x_{1A}	0.019319
x_{1B}	−0.572685
x_{2A}	−0.545886
x_{2B}	0.013334

This discussion suggests that we should be able to predict extinction probabilities from the composition of the population before the switch. We have fitted the probability p that a population becomes extinct after an antibiotic switch to a sigmoid function $p = (1+e^{\mathbf{W}^T\mathbf{N}})^{-1}$, where $\mathbf{W}$ is a parameter vector and $\mathbf{N} = (N_0, \ldots, N_3)$ contains the population abundances right before the antibiotic switch [Fig. 3(a), Appendix D]. The fitted parameters confirm our earlier intuition (Appendix D, Table II): p decreases when any genotype other than the single resistant increases. For example, if the population before the switch is $N_0 = 2$, $N_1 = 95$, $N_3 = 0$, then $p \approx 0.55$, but introducing one x_3 individual yields $p \approx 0.26$. This indicates that the extinction probability is largely determined by whether the population contains cells other than the currently dominant resistant genotype. The presence of even a small fraction of any other genotypes substantially decreases the chances of extinction.

However, it is unrealistic to assume that complete compositional data will be available in clinical or *in vitro* settings to decide when to switch antibiotics. We therefore propose a heuristic approach to approximate p using three key time distributions obtained from the dynamics of our four-genotype system. Specifically, we measured (1) the distribution of times for single-resistant mutants to dominate the population (defined as exceeding 80%) after an antibiotic switch; (2) the distribution of extinction times following an antibiotic switch; and (3) the probability that the population contains cells other than the single-resistant mutant for the antibiotic currently in use, a choice motivated by the sigmoid fit, as previously discussed.

The first two distributions were well-approximated by log-normal distributions (Fig. 4), and all three can in principle be measured *in vitro* to obtain a practical estimate of optimal switching strategies. Building on these distributions and the

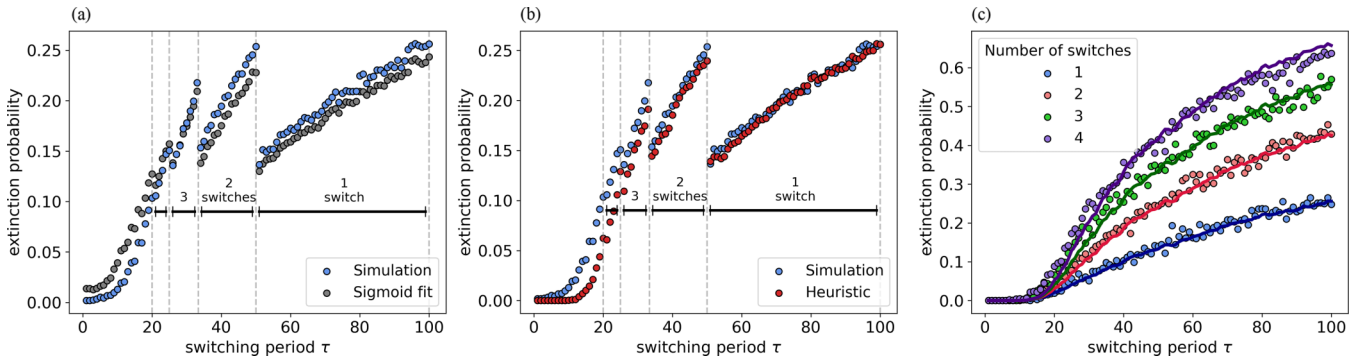

FIG. 3. Heuristic approximation for the extinction probability. (a) Sigmoid fit for the extinction probability at the end of the treatment, using the population composition before the switch. Blue circles represent the simulation; gray circles are the prediction of the sigmoid function fitted with the population before the switches. (b) Heuristic fit for the same probability as in (a) using fixed final time treatments, and considering several switching periods τ. (c) Heuristic fit for the extinction probability under different number of antibiotic switches. Circles are the values of extinction probabilities measured in simulations; each color represents a different number of antibiotic changes, as indicated in the legend. The solid lines indicate the estimated value of the probability of extinction for each τ, using the heuristic to estimate p. Parameter values are in Appendix B, Table I.

previous insights gained from our geometric model, we derived an analytical expression for the extinction probability p as a function of τ:

$$p(\tau) = p_d(\tau)[1 - p_r(\tau)], \tag{1}$$

where $p_d(\tau)$ is the probability that a decaying population becomes extinct within time τ [Fig. 4(b)], and $p_r(\tau)$ is the probability that a single-resistant mutant is not completely dominant in the population, given by

$$p_r(\tau) = p_{x_1}(\tau) \cdot \Pr\left(N_0 + N_2 + N_3 \geqslant 2 \mid \tau, N_2(0) = 90\right) + [1 - p_{x_1}(\tau)] \cdot \Pr\left(N_0 + N_2 + N_3 \geqslant 2 \mid \tau, N_0(0) = 50\right)$$

with $p_{x_1}(\tau)$ denoting the probability that genotype x_1 dominates the population at time τ, given that the system started with x_2 in dominance [Fig. 4(a)]. Intuitively, for short times the initial condition $N_0(0) = 50$ provides a good approximation, while for longer times the condition $N_2(0) = 90$ becomes more accurate. The weighting between these two scenarios is naturally captured by the distribution of takeover times of the single-resistant strain, represented by $p_{x_1}(\tau)$.

We use the geometric distribution formula to extend these extinction probabilities to various antibiotic changes. However, some care has to be taken with the initial and boundary conditions at the end of the treatment (Appendix E). This formula captures our previous intuitions for the two necessary conditions for extinction: the dominance of the single-resistant genotype and the existence of long enough decay times. This simple heuristic matches the shape of extinction probabilities derived from full stochastic simulations [Fig. 3(b)] and gives an accurate estimate for cumulative extinction probabilities of populations under one, two, or more antibiotic switches [Fig. 3(c)].

C. Additional scenarios: Weak collateral sensitivity, increasing antibiotic concentrations, and changing mutation rates

Our results so far have dealt with strong reciprocal CS, $k_{CS} = 0.05$. If the strength of CS diminishes (k_{CS} grows), the extinction probabilities at the end of the treatment decrease, as expected given the previous discussion [Fig. 5(a)]. Although

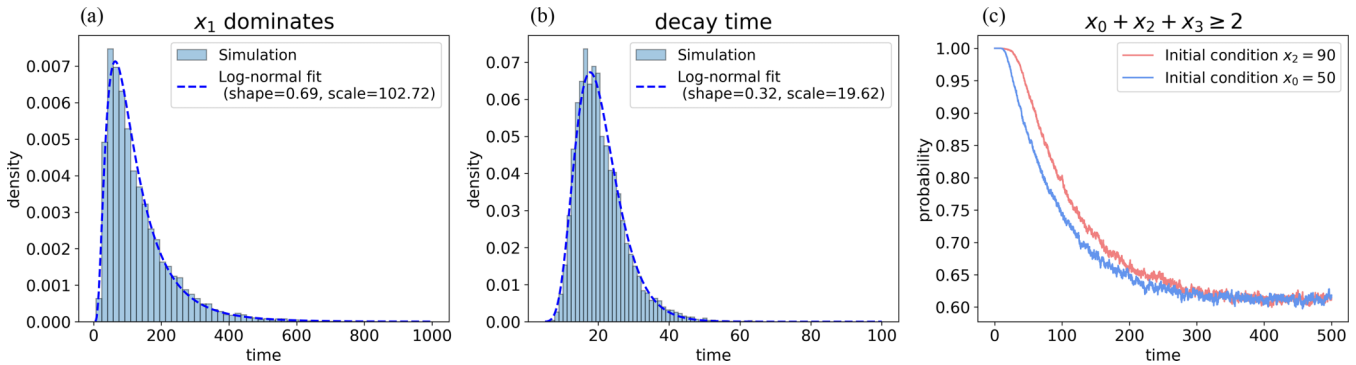

FIG. 4. Distributions for key transition times in the model. Simulated distributions (blue histograms) and fitted log-normal probability density functions (dashed curves) for two temporal processes underlying the heuristic extinction estimate. (a) Time until the system transitions between stable states following an antibiotic change, starting from $x_2(0) = 80$ and $x_i(0) = 0$ for $i = 0, 1, 3$ under antibiotic A until $x_1(t) > 80$. (b) Time to extinction under a new antibiotic, measured only for simulations where extinction occurs. (c) Time dependent probability of having $x_0 + x_2 + x_3 \geqslant 2$ starting from the initial conditions indicated by colors in the legend. 10 000 trajectories were simulated for estimating these distributions.

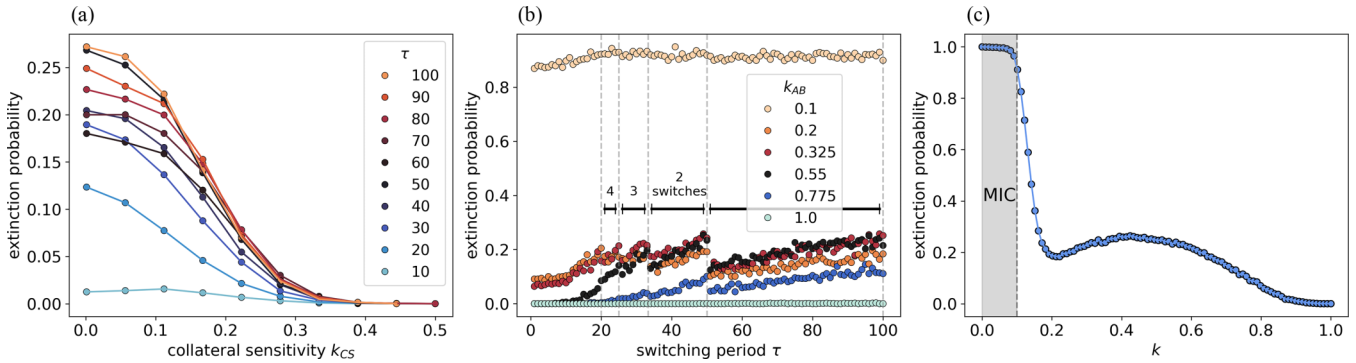

FIG. 5. Extinction probability sensitivity to model parameters. (a) Collateral sensitivity (CS) is necessary for extinction. Extinction probabilities decrease as the parameter k_{CS} increases, across a range of switching periods (τ, shown in color). (b) Increasing antibiotic concentration (lowering k) robustly leads to extinction, depending on the number of treatment cycles. We observe a threshold near the MIC, beyond which most populations become extinct regardless of the switching period. (c) Extinction probability as a function of antibiotic concentration for $\tau = 50$. Close to the MIC, every trajectory becomes extinct. For subinhibitory doses, there is an intermediate dose that maximizes extinction.

the dependence of extinction probability on τ is qualitatively similar, i.e., optimal τ remain the same throughout, the maximum extinction probability decreases monotonically as k_{CS} increases, and for $k_{CS} > 0.3$ it is approximately zero for all τ. That is, for subinhibitory concentrations, CS is a necessary condition for the success of sequential therapies.

We wondered then whether this dependency on CS would be weakened if we increased antibiotic doses. We reasoned that, as $k_A, k_B \to 0$, the total extinction probability should increase. For concentrations close to the minimum inhibitory concentration (MIC), i.e., $k = 0.1$ or lower, a threshold behavior emerges where populations go extinct regardless of the switching period [Figs. 5(b) and 5(c)], suggesting that extinction is driven primarily by the strength of inhibition rather than the switching dynamics. Indeed, this behavior persists even in the absence of CS (Appendix F, Fig. 12). However, for lower antibiotic concentrations $k > 0.1$ we observe a unimodal dependency of the extinction probability on the dose: for a fixed τ, extinction probabilities go up as we decrease k from 1, and then decrease after a certain dose [Figs. 5(b) and 5(c)]. We reason that this is due to a change in population dynamics: when antibiotic inhibition increases, the single-resistant mutant quickly dominates the population, which then becomes extinct more easily as we switch the antibiotic. However, if antibiotic inhibition crosses a given threshold, the wild-type population is so low that the influx of resistant mutants actually becomes slower, and therefore the population does not become extinct after switching. We support this qualitative reasoning looking at the mean population before the first switch (Appendix F, Fig. 13). In the same way, extinction probabilities show a unimodal dependency on mutation: as μ_1 increases, extinction probabilities go up, again due to an increase in the abundance of single-resistant mutants (Appendix F, Fig. 14). However, after a critical threshold, the extinction probability starts to decrease, in this case because the double-resistant strain emerges in the population, while the susceptible strain concurrently exhibits a recovery (Appendix F, Fig. 15). Moreover, as μ_2/μ_1 increases, the extinction probability decreases more markedly, which is consistent with the accelerated recovery of the susceptible strain under these conditions, since single-resistant mutants become less frequent when μ_2 is relatively larger.

D. Optimal switching periods

After providing an evolutionary population-dynamics argument for the success of sequential therapies based on strong reciprocal CS, and studying the effect of varying several parameters, we return to finding the optimal switching periods. So far, we have discussed optimality only in terms of maximizing the cumulative extinction probability at the end of the treatment. In mathematical terms, this function is $E(\tau, n) = 1 - [1 - p(\tau)]^n$ where $p(\tau)$ is an increasing function of τ, as we have discussed [Fig. 2(e)]. Therefore, $E(\tau, n)$ increases both with τ and with the number of switches n: if the population does not become extinct after the first change, it may do so after subsequent changes. In fact, for a fixed τ, the probability of extinction can increase as much as we want by increasing n [Fig. 6(a)].

However, this comes with a cost: longer therapies also have a higher probability that the double-resistant genotype x_3 appears in the population at the end of the treatment [Fig. 6(b)], so if the population is not extinct it will become resistant. Hence, there is a tradeoff between maximizing extinction probabilities and minimizing the probability of double-resistance, leading to a Pareto front of feasible therapies [Fig. 6(c)] that optimize both objectives. For a fixed extinction probability $E(\tau, n)$, the Pareto front contains those therapies that minimize the probability of double resistance at the end of the treatment, conditioned on the population not being extinct, which we define as $R(\tau, n) = \Pr(N_3(T) \geqslant 1 | N(T) > 0)$. If a therapy is not on the Pareto front, we can always modify it so that either $E(\tau, n)$ or $1 - R(\tau, n)$ are improved: they are *dominated* by other, better therapies. Crucially, therapies on the Pareto front cannot improve $E(\tau, n)$ without increasing $R(\tau, n)$ as well. We numerically find that the Pareto front is captured by the curve $E(\tau, n)^{1.09} + [1 - R(\tau, n)]^{1.22} = 1$ [Fig. 6(c)]. We can also show that the probability of being in the Pareto front is very high for $\tau \approx 42$ [Fig. 7(a)], independently of the number

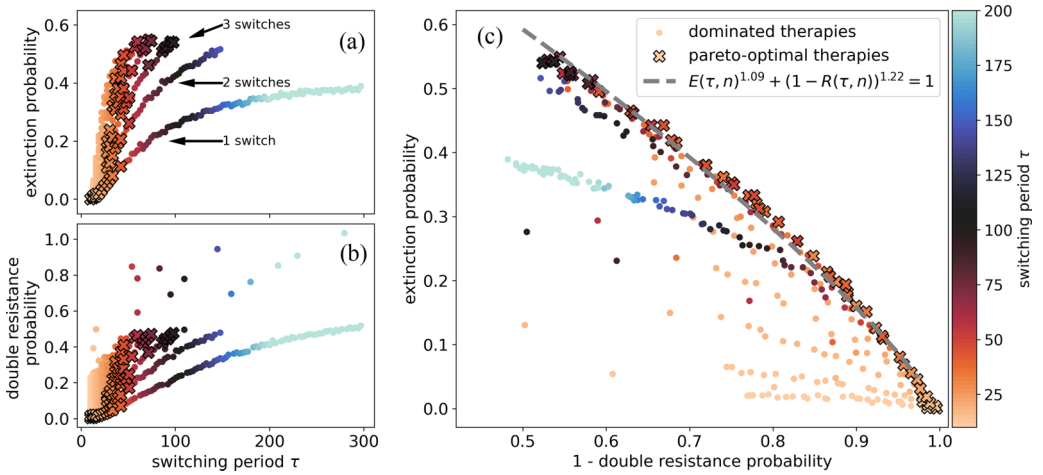

FIG. 6. Optimal therapy. (a) Extinction probability as a function of the switching period. (b) Probability of double resistant mutants at the end of the treatment, conditioned on the population not being extinct. (c) Pareto front of optimal switching therapies. The crosses indicate therapies that belong to the Pareto front, while the circles show dominated (suboptimal) therapies. The grey dashed line indicates the empirical fit. The probability that a therapy is in the Pareto front is maximized for $\tau \approx 42$. Simulated therapy trajectories were generated with different switching periods (τ) and numbers of treatment rounds (n), constrained such that $\tau n + 50 < 350$, number of trajectories $= 10\,000$, $k = 0.5$, $k_{\mathrm{CS}} = 0.05$.

of changes [Fig. 7(b)] and lower everywhere else. Hence, for the parameter set studied in this paper, choosing τ around that value will lead to optimal therapies: we can then choose whether we want to maximize extinction or minimize resistance by changing the number of switches n.

IV. DISCUSSION

The use of CS to design sequential therapies has received widespread attention in recent years [17,43]. The underlying rationale is that antibiotics can be used to steer populations toward genotypic states exhibiting CS, thereby increasing the efficacy of subsequent treatments [44]. In this work, we develop a simple mathematical framework that captures key features of sequential therapies, enabling quantitative exploration of extinction dynamics and providing support for prior evolutionary hypotheses. While experimental studies have demonstrated the potential of sequential therapies to suppress resistance [20,21,45], theoretical efforts have largely relied on deterministic models where extinctions do not occur [46–48], although a recent work has used stochastic modeling to explore the effect of antibiotic pulses [24]. In contrast to deterministic models, our stochastic modeling framework captures extinction dynamics directly. This enables the identification of optimal treatment strategies based on true eradication events and allows us to explore how extinction probabilities depend on switching timing, antibiotic potency, and mutation rates.

In [46], Beardmore and Peña-Miller state that a successful switching strategy, based on clinical observations [49], is "*if the observed level of resistance to an antibiotic is too high, exchange it for a different antibiotic*", which is fully consistent with our results. In fact, a key result from our analysis is that fast sequential therapies are suboptimal, and that we need to allow for the evolution of resistance above a threshold

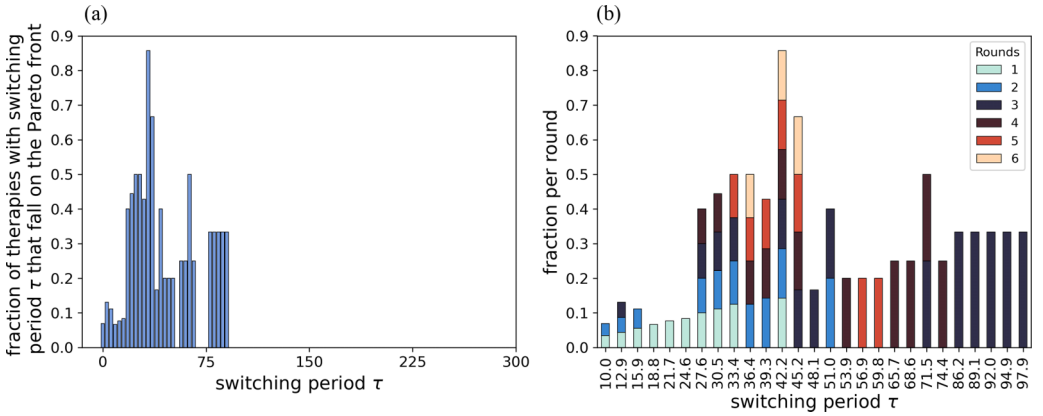

FIG. 7. Optimal window. Simulated therapy trajectories were generated with different switching periods (τ) and numbers of treatment rounds (n), constrained such that $\tau n + 50 < 350$. (a) Fraction of therapies with a given switching period τ that lie on the Pareto front. (b) Distribution of these fractions across the different numbers of treatment rounds. We observe that certain switching periods consistently fall on the Pareto front regardless of the number of rounds ($\tau \approx 42$), while others are optimal only for one ($\tau \approx 20$) or three ($\tau \approx 90$) switching events. Number of trajectories $= 10\,000$.

in order to eradicate the population after the switch. The tension between waiting long enough for the single-resistant mutant to dominate the population and maximizing the number of switches leads to different optimal switching periods depending on the treatment duration (Fig. 6): longer therapies maximize extinction, but they also cause higher resistance, leading to a Pareto front of optimal switching periods. This gives us some additional insight that will help to choose optimal therapies.

Furthermore, our framework demonstrates that while the requirement for strong CS is a necessary condition for causing extinctions, it allows sequential therapies to outperform traditional monotherapy. In regimes where the antibiotic dose is high, extinction occurs reliably regardless of the switching period [Fig. 5(b)]. However, the true strength of this approach lies in its efficacy under subinhibitory concentrations, conditions that are clinically inevitable due to drug diffusion limits within human tissues [50]. In these suboptimal dosage zones, where no-switching treatments fail, our model shows that an optimized sequential protocol can still drive the population to extinction.

In addition, we find a unimodal dose-extinction relationship [Fig. 5(c)], which has been observed before in both experiments [42] and models [51] and which can be fully explained using population dynamics arguments: we need single-resistant mutants to dominate the population; these are selected as antibiotic concentration increases, but selection can be hampered if doses are too high. We observe a similar relationship with mutation rates (Appendix F, Fig. 14), also supported by population dynamics arguments. This result suggests that increasing mutation rates might be a good complement to this kind of therapies, up to a point where we start facilitating the evolution of double-resistant strains. This suggestive strategy should be explored with care and checked experimentally before making any therapy recommendations.

This study adopts a deliberately minimal within-host model, four genotypes and two antibiotics with symmetric effects, to isolate the mechanisms of CS-guided switching. Extensions to richer collateral-sensitivity networks [17–19] and to heterogeneous pharmacokinetics/pharmacodynamics [48] fit naturally within the same framework. CS relationships may vary during treatment [52–54]; such time dependence can be incorporated by allowing parameters to evolve between switches and calibrating them from data. Empirical evaluation can proceed *in vitro* without altering the theoretical structure. A suitable test system is the ciprofloxacin-tobramycin pair in *P. aeruginosa*, where CS has been observed robustly, and double resistance is infrequent [19,55,56], enabling direct assessment of the model's predictions.

Our model admits several avenues for generalization beyond the present focus. Beyond bacteria, the mathematical structure of our framework maps naturally onto cancer, where CS has been documented across multiple tumor types and treatment classes [57–60]. Sequential exploitation of these tradeoffs has been proposed as a strategy to steer tumor clonal evolution toward more vulnerable states [59], and experimental evidence using cellular barcoding has identified CS drugs following resistance to chemotherapy in colorectal cancer cell lines [61]. More broadly, the adaptive therapy framework [62,63] exploits analogous competitive dynamics between sensitive and resistant subpopulations under modulated treatment schedules, and has been extended to multidrug sequential protocols [63] that share the same underlying logic as our model.

Although our focus is on short-term antibiotic treatments, our framework could naturally be applied to chronic infections, where treatment timescales are prolonged and resistance fixation is a central clinical problem. Indeed, sequential therapies have been proposed to treat chronic *Pseudomonas* lung infections where biofilm formation hinders the effectiveness of monotherapies [64,65].

The model could also be lifted to the epidemiological scale, to account transmission dynamics within a population of patients [29–31]. Such extension would introduce additional characteristic timescales, governed by host-to-host interaction frequencies and the mechanisms of transmission, that are qualitatively distinct from the within-host evolutionary dynamics studied here, and might open the possibility of population-level treatment strategies that are not optimal for the individual.

Beyond periodic schedules, our framework can be extended to nonperiodic and adaptive switching policies as considered in [46,47]. Because we treat therapy as a series of switches, each a fresh chance to clear the infection, the same framework lends itself to control-theoretic optimization of switching sequences, including real-time, patient-specific adjustments informed by bacterial-load measurements.

Overall, these results provide quantitative design rules for sequential therapy guided by collateral sensitivity and mathematical modeling, complementing current strategies against antimicrobial resistance.

ACKNOWLEDGMENTS

We thank all members of the Ares-Catalán laboratory for fruitful discussions, in particular Lucía Yubero for her detailed review of the sigmoid fit. This research was funded by the Spanish Ministerio de Ciencia e Innovación (MCIN/AEI/10.13039/501100011033) and by ERDF/EU "A way of making Europe" through grant PGE, Grants No. PID2022-142185NB-C21 (S.A.) and No. PID2022-142185NB-C22 (P.C.); grant BASIC, Grant No. PID2022-141802NB-I00 (J.A.C.); and grant GALAR, Grant No. PID2022-138916NB-I00 (B.P.-E.). The CNB-CSIC is further supported by a Severo Ochoa Excellence grant (CEX2023-001386-S funded by MICIU/AEI/10.13039/501100011033).

DATA AVAILABILITY

The data that support the findings of this article are openly available [66].

APPENDIX A: JUSTIFICATION FOR THE POPULATION THRESHOLD AND TAU-LEAPING APPROXIMATION

In the main text, we considered a stochastic model of bacterial population dynamics under antibiotic treatment, where extinction was defined as the population dropping below a threshold of $0.05\gamma^{-1} = 5$ individuals. Simulations were performed using the tau-leaping method to efficiently approximate the stochastic process. Here, we justify this approach by

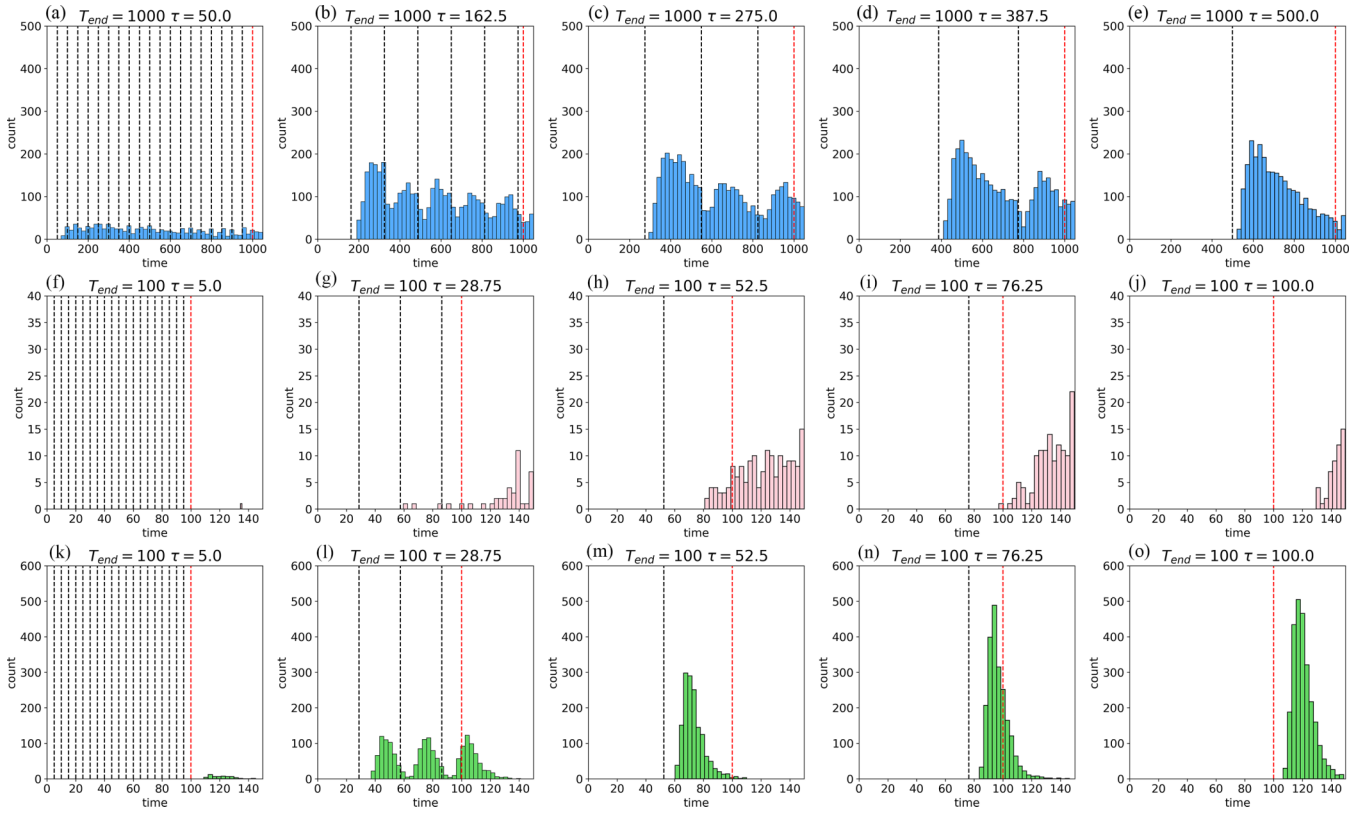

FIG. 8. Extinction histograms for the hybrid method: Tau leaping and Gillespie's algorithm. The top row (blue) shows extinction histograms with a total time of $t_{\text{end treatment}} = 1000$ and $t_{\text{end}} = 1050$ temporal units. As the antibiotic switching interval increases, extinction events become more clearly clustered after switching events (dashed black vertical lines). Dashed red vertical lines indicate $t_{\text{end treatment}}$. The middle row (pink) presents extinction histograms for a shorter total simulation time of $t_{\text{end treatment}} = 100$ and $t_{\text{end}} = 150$ temporal units, the same temporal scale used in the main text. At this scale, extinction events appear more diffusely distributed, making it difficult to discern their relationship with antibiotic changes. Both (blue and pink) consider extinction when the number of cells in the population is zero, and switch between tau leaping and Gillespie's algorithm with a threshold of 10 cells. The bottom row (green) shows results from Gillespie's algorithm with a threshold of $0.05/\gamma$ for extinction and 15 cells for switching between tau leaping and Gillespie, the total simulation time of $t_{\text{end treatment}} = 100$ and $t_{\text{end}} = 150$ temporal units. The results are consistent with those observed with tau leaping, supporting the strategy used throughout the main text.

comparing it with a hybrid method that uses tau leaping for populations with many individuals and Gillespie's algorithm for populations below that limit. Gillespie's algorithm provides an exact simulation of the underlying stochastic process but becomes computationally prohibitive when population size is large. Specifically, as the number of bacteria increases, the waiting times between reaction events shorten, leading to a significant increase in computational cost. This has a direct impact on the feasibility of simulating extinction events under different antibiotic switching strategies.

To assess whether the chosen threshold and tau-leaping approximation capture the relevant extinction dynamics, we performed simulations using the hybrid method and compared the results. Our key observation is that extinction events occur primarily after an antibiotic switch, with a characteristic delay. However, when antibiotic switching times are of the same order of magnitude as reaction times at low population sizes, this pattern is no longer evident. Instead, we observe a diffuse cloud of extinction events, making it difficult to distinguish the effect of antibiotic changes. To recover the expected correlation between switching events and extinctions, it is necessary to increase the switching times.

To illustrate these findings, we present extinction histograms from three sets of simulations. The first set (Fig. 8, top row) corresponds to a longer total simulation time of 1000 temporal units, allowing for a clearer observation of extinction clustering after antibiotic switches. The second set (Fig. 8, middle row) corresponds to a shorter total simulation time of 100 temporal units, matching the temporal scale used in the main text. In this shorter time frame, extinction events appear as a diffuse pattern, making it harder to discern correlations with antibiotic changes. In contrast, with a sufficiently long observation window, the extinction events align with antibiotic switching events, confirming that the primary driver of extinction is the switching strategy itself. In these two sets, we have considered extinctions when we have a population of zero bacteria. We add a third set using the hybrid method but with the same threshold for the extinctions used in the main text (Fig. 8, bottom row), confirming that the results are consistent and that the tau-leaping algorithm does not qualitatively alter the observed patterns.

We also compared the distribution of extinction times for fast-extinction events (such as those involving a high antibiotic dose, $\kappa = 0.1$) and observed an overlap between the two histograms. This makes the tau-leaping approximation also a

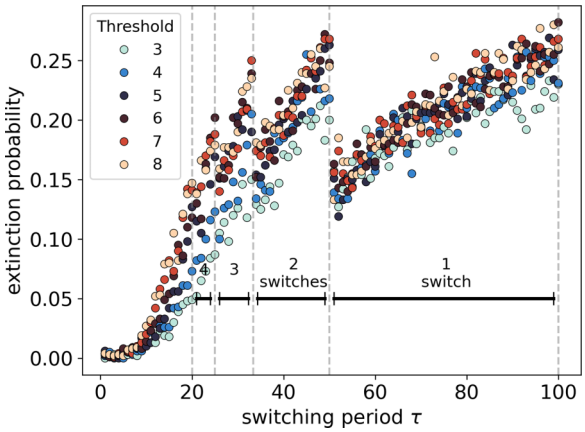

FIG. 9. Changing the extinction threshold does not change the qualitative behavior of the extinction curve. Different thresholds for determining when a population is considered to be extinct, from 3% to 8% of theoretical carrying capacity. In the main text 5% has been used as the threshold.

good approximation of the solution to the master equation in this regime.

Finally, we tested the robustness of the extinction threshold. In the main text, we consider a population extinct if it goes below 5% carrying capacity. We varied this threshold between 3% and 8% and obtained quantitatively very similar results (Fig. 9).

APPENDIX B: PARAMETERS USED IN THE MAIN TEXT

Unless otherwise stated, all graphs in the main text were made with the parameter values in Table I.

APPENDIX C: NONEQUILIBRIUM EFFECTS AND A HIERARCHICAL GEOMETRIC MODEL

The discrepancies observed in the geometric model fit from Figs. 10(a) and 10(b) can be explained by the fact that the system is not in equilibrium. To better understand this behavior, we analyzed the extinction probability per round, p, as a function of time and the number of rounds. We performed a linear fit of the form $p = \alpha\tau + \beta n$, where p is the extinction probability, τ is the switching period, and n is the number of completed treatment rounds [Fig. 10(c)]. This model captures the systematic dependence of extinction dynamics on both time and the structure of the treatment.

We then used this time-dependent extinction probability to construct a hierarchical geometric model for the cumulative extinction probability:

$$P_{\text{ext}} = 1 - (1 - \alpha\tau - \beta n)^n,$$

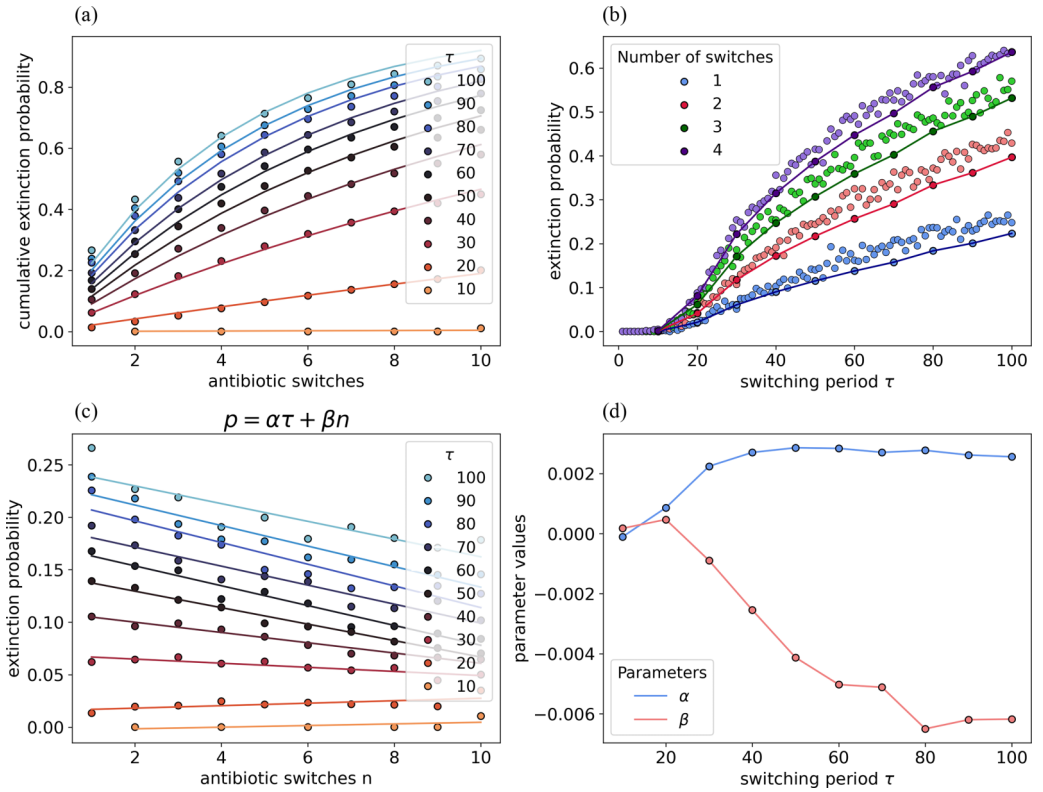

FIG. 10. (a) Cumulative extinction probability over 10 treatment switches with different switching periods τ. Points represent extinction probabilities estimated through simulation, while the solid line reflects a fit to a geometric distribution $1 - (1 - p)^n$. (b) Estimation of the extinction probability for different number of antibiotic switches (represented with colors as indicated in the legend) using the fit of the geometric model obtained in (a). (c) Linear fit to the extinction probability after each switch for the hierarchical geometric model. (d) Estimated parameters for each τ in (c).

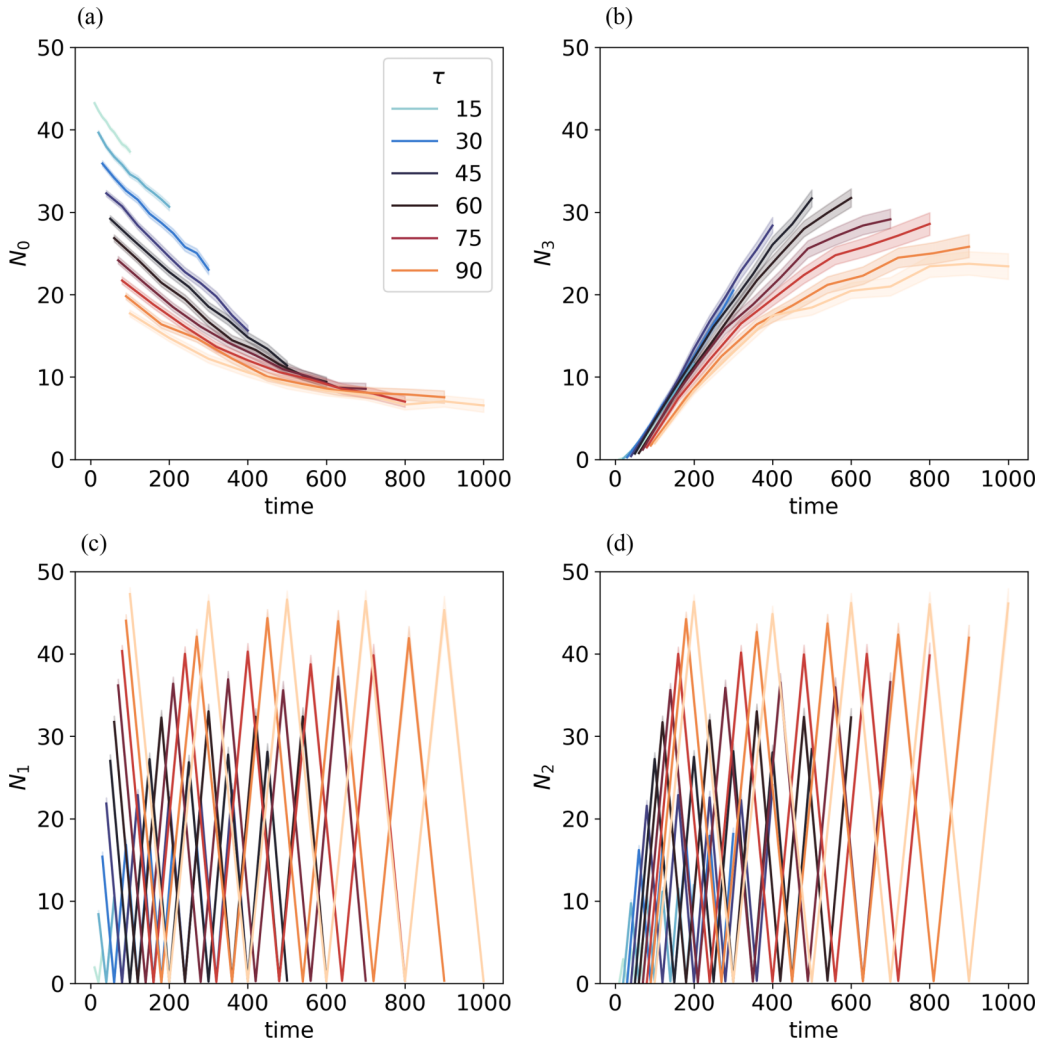

FIG. 11. Mean population trajectories. Mean values of the trajectories before the switch simulated for the geometric fit. Shades indicate 95% confidence interval. We observe that surviving populations achieve double-resistant mutants. (a) N_0. (b) N_3. (c) N_1 oscillatory behavior. (d) N_2 oscillatory behavior.

which fits the data well over a wide range of conditions [Fig. 2(d)].

To explore how the fitting parameters vary with the switching period, we examined the dependence of α and β on τ [Fig. 10(d)]. For small values of τ, we find $\beta > 0$, indicating that the probability of extinction increases with the number of rounds. This could be due to the oscillatory regime driving the system into extinction-prone states. In contrast, for large τ, we observe $\beta < 0$, suggesting that prolonged exposure in each cycle may favor the emergence of double-resistant mutants, reducing extinction probability over time (Fig. 11). Together, these results highlight the importance of nonequilibrium effects in shaping extinction outcomes during sequential therapy.

APPENDIX D: PARAMETERS OF THE SIGMOID FIT

We introduce as parameters to be adjusted in a logistic model the population before the change of antibiotic. Depending on the antibiotic we are using, the populations of x_1 and x_2 have different growth rates, and therefore we consider the variables

$$x_{iA} = 0 \quad \text{if antibiotic is } B, \quad x_i \text{ otherwise},$$
$$x_{iB} = x_i \quad \text{if antibiotic is } B, \quad 0 \text{ otherwise}$$

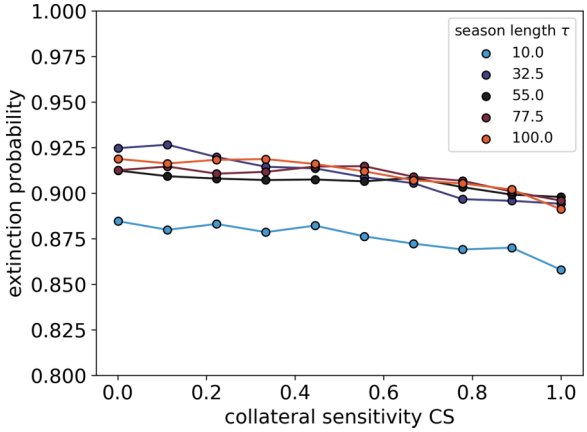

FIG. 12. Collateral sensitivity is irrelevant when high doses of antibiotic are applied. Simulations with $k = 0.1$.

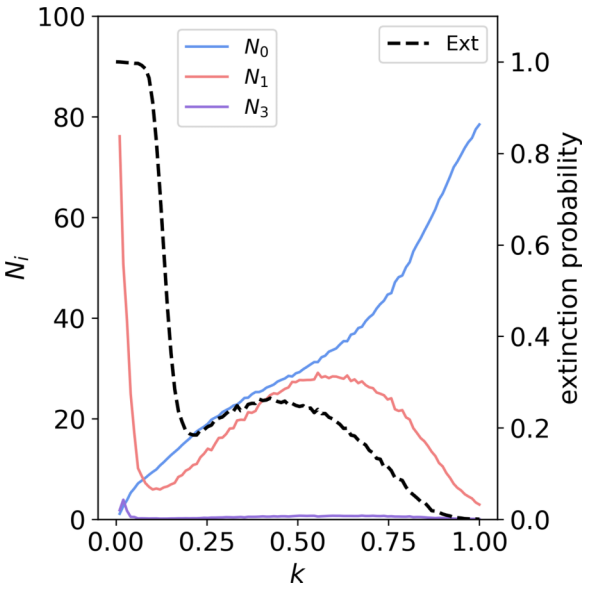

FIG. 13. Effect of changes in antibiotic concentration. Mean population composition prior to the first switch (colored lines), superimposed with the extinction probability (black dashed line). As antibiotic inhibition increases (k decreases), the population of x_1 goes up, which leads to an increase in extinction probability. After a certain antibiotic concentration (below $k \approx 0.7$), x_0 does not reach high values, and evolution to x_1 slows down. This leads to a decrease in extinction at intermediate to high antibiotic concentrations ($k < 0.4$ approximately). When antibiotic inhibition becomes very strong (i.e., $k < 0.1$), the decrease in x_0 is so strong that populations become extinct not due to collateral sensitivity, but because the overall carrying capacity is very low and extinctions occur from fluctuations. Simulations with $\tau = 50$, $t_{\text{end}} = 150$, $t_{\text{end treatment}} = 100$, number of trajectories $= 10\,000$.

for $i = 1, 2$. We therefore end up with the following inputs: $x_0, x_3, x_{1A}, x_{1B}, x_{2A}, x_{2B}$ (Table II).

We observed that having x_0 or x_3 in the population before the switch reduces the probability of extinction (the parame-

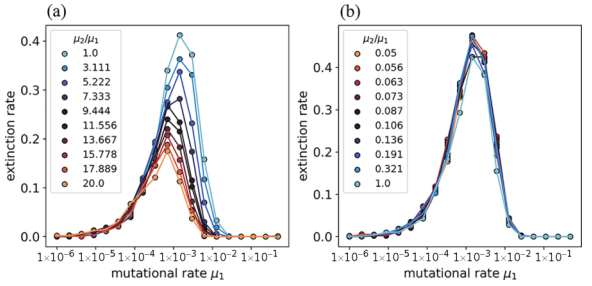

FIG. 14. Effect of changes in mutation rates. (a) Extinction rate as a function of mutation rate μ_1, for a range of ratios μ_2/μ_1 ranging from 1 to 20 (see legend), i.e. $\mu_2 \geqslant \mu_1$. (b) Same as (a) but the ratio μ_2/μ_1 now goes from 0.05 to 1 (see legend), i.e. $\mu_1 > \mu_2$. The extinction probability exhibits a nonmonotonic dependence on the baseline mutation rate (μ_1), peaking at intermediate values. The ratio between mutation rates μ_2/μ_1 modulates the peak height and position, but does not otherwise alter this behavior. Simulations with $\tau = 50$, $t_{\text{end}} = 150$, $t_{\text{end treatment}} = 100$, number of trajectories $= 1000$.

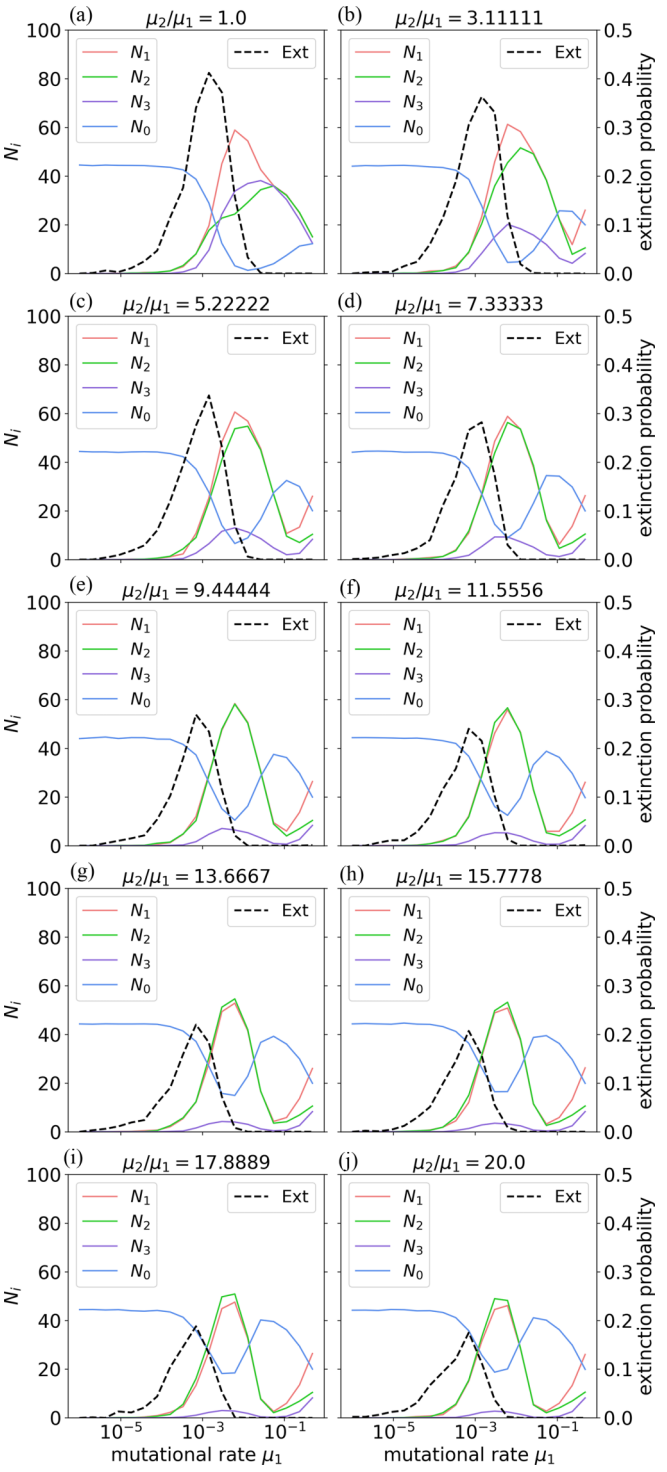

FIG. 15. Effect of changes in mutation rates. Mean population composition prior to the switch for trajectories that do not become extinct (colored lines), and extinction probability (black dashed line). The decline of the extinction peak coincides with the emergence of the double-resistant strain and with the recovery of the susceptible strain, the latter becoming more pronounced as μ_2 increases relative to μ_1. $\tau = 50$, $t_{\text{end}} = 150$, $t_{\text{end treatment}} = 100$, number of trajectories $= 1000$.

ters are negative). The same happens when we have bacteria that will be resistant after switching, x_{1B} and x_{2A}. The best scenario for extinction is when all the population is dominated by either x_{1A} or x_{2B}. The dataset used for these fits is the population composition before the switch of 10 000 trajectories per τ simulated to estimate the extinction probability of Fig. 2(a).

APPENDIX E: FORMULA FOR THE EXTENSION OF THE HEURISTIC

Due to the boundary and initial conditions, Eq. (1) in the main text cannot be introduced directly into the geometric distribution for extending the extinction probability to multiple switches. Remember that $p(\tau)$ has two contributions: $p_r(\tau)$, the probability that the single-resistant mutant is not completely dominant in the population, and $p_d(\tau)$, the probability that a population gets extinct in a time smaller than τ.

For the first antibiotic switch $p_{\text{init}}(\tau)$, we calculate $p_{r,\text{init}}(\tau)$ as

$$p_{r,\text{init}}(\tau) = \Pr[x_0 + x_2 + x_3 \geqslant 2|\tau, x_0(0) = 50].$$

Similarly, after the last antibiotic switch, $p_{\text{bound}}(\tau)$, we modify the decay probability to $p_{d,\text{bound}} = p_d(t_{\text{end}}(\text{mod}\tau + 50))$, because the population has more time to decay, as a consequence of the chosen boundary conditions.

Putting everything together, we have the formula

$$p_{\text{ext}}(\tau) = 1 - [1 - p(\tau)]^{n-2}[1 - p_{\text{init}}(\tau)][1 - p_{\text{bound}}(\tau)].$$

APPENDIX F: SUPPLEMENTARY FIGURES

Figures 12–15 contain supplementary information referred to in the main text.

[1] P. Catalán, E. Wood, J. M. Blair, I. Gudelj, J. R. Iredell, and R. E. Beardmore, Seeking patterns of antibiotic resistance in ATLAS, an open, raw MIC database with patient metadata, Nat. Commun. **13**, 2917 (2022).

[2] M. Naghavi, S. E. Vollset, K. S. Ikuta, L. R. Swetschinski, A. P. Gray, E. E. Wool, G. R. Aguilar, T. Mestrovic, G. Smith, C. Han, *et al.*, Global burden of bacterial antimicrobial resistance 1990–2021: A systematic analysis with forecasts to 2050, Lancet **404**, 1199 (2024).

[3] M. Miethke, M. Pieroni, T. Weber, M. Brönstrup, P. Hammann, L. Halby, P. B. Arimondo, P. Glaser, B. Aigle, H. B. Bode, *et al.*, Towards the sustainable discovery and development of new antibiotics, Nat. Rev. Chem. **5**, 726 (2021).

[4] G. Liu, D. B. Catacutan, K. Rathod, K. Swanson, W. Jin, J. C. Mohammed, A. Chiappino-Pepe, S. A. Syed, M. Fragis, K. Rachwalski, *et al.*, Deep learning-guided discovery of an antibiotic targeting *Acinetobacter baumannii*, Nat. Chem. Biol. **19**, 1342 (2023).

[5] A. Martins, F. Judák, Z. Farkas, P. Szili, G. Grézal, B. Csörgő, M. S. Czikkely, E. Maharramov, L. Daruka, R. Spohn, *et al.*, Antibiotic candidates for Gram-positive bacterial infections induce multidrug resistance, Sci. Transl. Med. **17**, eadl2103 (2025).

[6] L. Daruka, M. S. Czikkely, P. Szili, Z. Farkas, D. Balogh, G. Grézal, E. Maharramov, T.-H. Vu, L. Sipos, S. Juhász, *et al.*, ESKAPE pathogens rapidly develop resistance against antibiotics in development in vitro, Nat. Microbiol. **10**, 313 (2025).

[7] M. Baym, L. K. Stone, and R. Kishony, Multidrug evolutionary strategies to reverse antibiotic resistance, Science **351**, aad3292 (2016).

[8] M. Tyers and G. D. Wright, Drug combinations: A strategy to extend the life of antibiotics in the 21st century, Nat. Rev. Microbiol. **17**, 141 (2019).

[9] R. Roemhild, T. Bollenbach, and D. I. Andersson, The physiology and genetics of bacterial responses to antibiotic combinations, Nat. Rev. Microbiol. **20**, 478 (2022).

[10] C. E. Rosenkilde, C. Munck, A. Porse, M. Linkevicius, D. I. Andersson, and M. O. Sommer, Collateral sensitivity constrains resistance evolution of the CTX-M-15 β-lactamase, Nat. Commun. **10**, 618 (2019).

[11] B. Kavčič, G. Tkačik, and T. Bollenbach, Mechanisms of drug interactions between translation-inhibiting antibiotics, Nat. Commun. **11**, 4013 (2020).

[12] P. D. Tamma, S. E. Cosgrove, and L. L. Maragakis, Combination therapy for treatment of infections with Gram-negative bacteria, Clin. Microbiol. Rev. **25**, 450 (2012).

[13] R. Pena-Miller, D. Laehnemann, G. Jansen, A. Fuentes-Hernandez, P. Rosenstiel, H. Schulenburg, and R. Beardmore, When the most potent combination of antibiotics selects for the greatest bacterial load: The smile-frown transition, PLoS Biol. **11**, e1001540 (2013).

[14] M. Vestergaard, W. Paulander, R. L. Marvig, J. Clasen, N. Jochumsen, S. Molin, L. Jelsbak, H. Ingmer, and A. Folkesson, Antibiotic combination therapy can select for broad-spectrum multidrug resistance in *Pseudomonas aeruginosa*, Int. J. Antimicrob. Agents **47**, 48 (2016).

[15] R. Roemhild and H. Schulenburg, Evolutionary ecology meets the antibiotic crisis: Can we control pathogen adaptation through sequential therapy? Evol. Med. Public Health **2019**, 37 (2019).

[16] C. Barbosa, V. Trebosc, C. Kemmer, P. Rosenstiel, R. Beardmore, H. Schulenburg, and G. Jansen, Alternative evolutionary paths to bacterial antibiotic resistance cause distinct collateral effects, Mol. Biol. Evol. **34**, 2229 (2017).

[17] L. Imamovic, M. M. H. Ellabaan, A. M. D. Machado, L. Citterio, T. Wulff, S. Molin, H. K. Johansen, and M. O. A. Sommer, Drug-driven phenotypic convergence supports rational treatment strategies of chronic infections, Cell **172**, 121 (2018).

[18] N. L. Podnecky, E. G. Fredheim, J. Kloos, V. Sørum, R. Primicerio, A. P. Roberts, D. E. Rozen, Ø. Samuelsen, and P. J. Johnsen, Conserved collateral antibiotic susceptibility networks in diverse clinical strains of *Escherichia coli*, Nat. Commun. **9**, 3673 (2018).

[19] S. Hernando-Amado, F. Sanz-García, and J. L. Martínez, Rapid and robust evolution of collateral sensitivity in *Pseudomonas aeruginosa* antibiotic-resistant mutants, Sci. Adv. **6**, eaba5493 (2020).

[20] A. Fuentes-Hernandez, J. Plucain, F. Gori, R. Pena-Miller, C. Reding, G. Jansen, H. Schulenburg, I. Gudelj, and R.

Beardmore, Using a sequential regimen to eliminate bacteria at sublethal antibiotic dosages, PLoS Biol. **13**, e1002104 (2015).
[21] A. Batra, R. Roemhild, E. Rousseau, S. Franzenburg, S. Niemann, and H. Schulenburg, High potency of sequential therapy with only β-lactam antibiotics, eLife **10**, e68876 (2021).
[22] R. E. Beardmore, R. Peña-Miller, F. Gori, and J. Iredell, Antibiotic cycling and antibiotic mixing: Which one best mitigates antibiotic resistance? Mol. Biol. Evol. **34**, 802 (2017).
[23] J. Maltas and K. B. Wood, Pervasive and diverse collateral sensitivity profiles inform optimal strategies to limit antibiotic resistance, PLoS Biol. **17**, e3000515 (2019).
[24] B. Morsky and D. C. Vural, Suppressing evolution of antibiotic resistance through environmental switching, Theor. Ecol. **15**, 115 (2022).
[25] G. Katriel, Optimizing antimicrobial treatment schedules: Some fundamental analytical results, Bull. Math. Biol. **86**, 1 (2024).
[26] D. T. Weaver, E. S. King, J. Maltas, and J. G. Scott, Reinforcement learning informs optimal treatment strategies to limit antibiotic resistance, Proc. Natl. Acad. Sci. USA **121**, e2303165121 (2024).
[27] J. Maltas, A. Huynh, and K. B. Wood, Dynamic collateral sensitivity profiles highlight opportunities and challenges for optimizing antibiotic treatments, PLoS Biol. **23**, e3002970 (2025).
[28] L. B. Aulin, A. Liakopoulos, P. H. van der Graaf, D. E. Rozen, and J. C. van Hasselt, Design principles of collateral sensitivity-based dosing strategies, Nat. Commun. **12**, 5691 (2021).
[29] S. Bonhoeffer, M. Lipsitch, and B. R. Levin, Evaluating treatment protocols to prevent antibiotic resistance, Proc. Natl. Acad. Sci. USA **94**, 12106 (1997).
[30] D. C. Angst, B. Tepekule, L. Sun, B. Bogos, and S. Bonhoeffer, Comparing treatment strategies to reduce antibiotic resistance in an in vitro epidemiological setting, Proc. Natl. Acad. Sci. USA **118**, e2023467118 (2021).
[31] M. Muetter, D. C. Angst, R. R. Regoes, and S. Bonhoeffer, The impact of treatment strategies on the epidemiological dynamics of plasmid-conferred antibiotic resistance, Proc. Natl. Acad. Sci. USA **121**, e2406818121 (2024).
[32] M. J. Shepherd, T. Fu, N. E. Harrington, A. Kottara, K. Cagney, J. D. Chalmers, S. Paterson, J. L. Fothergill, and M. A. Brockhurst, Ecological and evolutionary mechanisms driving within-patient emergence of antimicrobial resistance, Nat. Rev. Microbiol. **22**, 650 (2024).
[33] M. M. Mwangi, S. W. Wu, Y. Zhou, K. Sieradzki, H. de Lencastre, P. Richardson, D. Bruce, E. Rubin, E. Myers, E. D. Siggia, *et al.*, Tracking the *in vivo* evolution of multidrug resistance in *Staphylococcus aureus* by whole-genome sequencing, Proc. Natl. Acad. Sci. USA **104**, 9451 (2007).
[34] J. M. Blair, V. N. Bavro, V. Ricci, N. Modi, P. Cacciotto, U. Kleinekathöfer, P. Ruggerone, A. V. Vargiu, A. J. Baylay, H. E. Smith, *et al.*, AcrB drug-binding pocket substitution confers clinically relevant resistance and altered substrate specificity, Proc. Natl. Acad. Sci. USA **112**, 3511 (2015).
[35] R. Wheatley, J. D. Caballero, N. Kapel, F. H. R. de Winter, P. Jangir, A. Quinn, E. del Barrio-Tofiño, C. López-Causapé, J. Hedge, G. Torrens, *et al.*, Rapid evolution and host immunity drive the rise and fall of carbapenem resistance during an acute *Pseudomonas aeruginosa* infection, Nat. Commun. **12**, 2460 (2021).
[36] H. Chung, C. Merakou, M. M. Schaefers, K. B. Flett, S. Martini, R. Lu, J. A. Blumenthal, S. S. Webster, A. R. Cross, R. Al Ahmar, *et al.*, Rapid expansion and extinction of antibiotic resistance mutations during treatment of acute bacterial respiratory infections, Nat. Commun. **13**, 1231 (2022).
[37] T. Gil-Gil, B. A. Berryhill, J. A. Manuel, A. P. Smith, I. C. McCall, F. Baquero, and B. R. Levin, The evolution of heteroresistance via small colony variants in *Escherichia coli* following long-term exposure to bacteriostatic antibiotics, Nat. Commun. **15**, 7936 (2024).
[38] D. T. Gillespie, Stochastic simulation of chemical kinetics, Annu. Rev. Phys. Chem. **58**, 35 (2007).
[39] D. T. Gillespie, A general method for numerically simulating the stochastic time evolution of coupled chemical reactions, J. Comput. Phys. **22**, 403 (1976).
[40] P. Ankomah and B. R. Levin, Exploring the collaboration between antibiotics and the immune response in the treatment of acute, self-limiting infections, Proc. Natl. Acad. Sci. USA **111**, 8331 (2014).
[41] D. I. Andersson and D. Hughes, Evolution of antibiotic resistance at non-lethal drug concentrations, Drug Resist. Updat. **15**, 162 (2012).
[42] C. Reding, P. Catalán, G. Jansen, T. Bergmiller, E. Wood, P. Rosenstiel, H. Schulenburg, I. Gudelj, and R. Beardmore, The antibiotic dosage of fastest resistance evolution: Gene amplifications underpinning the inverted-U, Mol. Biol. Evol. **38**, 3847 (2021).
[43] F. Sanz-García, T. Gil-Gil, P. Laborda, P. Blanco, L.-E. Ochoa-Sánchez, F. Baquero, J. L. Martínez, and S. Hernando-Amado, Translating eco-evolutionary biology into therapy to tackle antibiotic resistance, Nat. Rev. Microbiol. **21**, 671 (2023).
[44] D. Nichol, P. Jeavons, A. G. Fletcher, R. A. Bonomo, P. K. Maini, J. L. Paul, R. A. Gatenby, A. R. Anderson, and J. G. Scott, Steering evolution with sequential therapy to prevent the emergence of bacterial antibiotic resistance, PLoS Comput. Biol. **11**, e1004493 (2015).
[45] R. Roemhild, C. S. Gokhale, P. Dirksen, C. Blake, P. Rosenstiel, A. Traulsen, D. I. Andersson, and H. Schulenburg, Cellular hysteresis as a principle to maximize the efficacy of antibiotic therapy, Proc. Natl. Acad. Sci. USA **115**, 9767 (2018).
[46] R. E. Beardmore and R. Peña-Miller, Rotating antibiotics selects optimally against antibiotic resistance, in theory, Math. Biosci. Eng. **7**, 527 (2010).
[47] R. Beardmore and R. Pena-Miller, Antibiotic cycling versus mixing: The difficulty of using mathematical models to definitively quantify their relative merits, Math. Biosci. Eng. **7**, 923 (2010).
[48] C. Nyhoegen and H. Uecker, Sequential antibiotic therapy in the laboratory and in the patient, J. R. Soc. Interface **20**, 20220793 (2023).
[49] B. Allegranzi, R. Luzzati, A. Luzzani, F. Girardini, L. Antozzi, R. Raiteri, G. Di Perri, and E. Concia, Impact of antibiotic changes in empirical therapy on antimicrobial resistance in intensive care unit-acquired infections, J. Hosp. Infect. **52**, 136 (2002).
[50] M. Müller, A. dela Peña, and H. Derendorf, Issues in pharmacokinetics and pharmacodynamics of anti-infective agents: Distribution in tissue, Antimicrob. Agents Chemother. **48**, 1441 (2004).

[51] P. Czuppon, T. Day, F. Débarre, and F. Blanquart, A stochastic analysis of the interplay between antibiotic dose, mode of action, and bacterial competition in the evolution of antibiotic resistance, PLoS Comput. Biol. **19**, e1011364 (2023).

[52] M. Yoshida, S. G. Reyes, S. Tsuda, T. Horinouchi, C. Furusawa, and L. Cronin, Time-programmable drug dosing allows the manipulation, suppression and reversal of antibiotic drug resistance *in vitro*, Nat. Commun. **8**, 15589 (2017).

[53] C. Barbosa, R. Römhild, P. Rosenstiel, and H. Schulenburg, Evolutionary stability of collateral sensitivity to antibiotics in the model pathogen *Pseudomonas aeruginosa*, eLife **8**, e51481 (2019).

[54] V. Sørum, E. L. Øynes, A. S. Møller, K. Harms, Ø. Samuelsen, N. L. Podnecky, and P. J. Johnsen, Evolutionary instability of collateral susceptibility networks in ciprofloxacin-resistant clinical *Escherichia coli* strains, mBio **13**, e0044122 (2022).

[55] S. Hernando-Amado, C. López-Causapé, P. Laborda, F. Sanz-García, A. Oliver, and J. L. Martínez, Rapid phenotypic convergence towards collateral sensitivity in clinical isolates of *Pseudomonas aeruginosa* presenting different genomic backgrounds, Microbiol. Spectr. **11**, e02276-22 (2023).

[56] S. Hernando-Amado, P. Laborda, R. La Rosa, S. Molin, H. K. Johansen, and J. L. Martínez, Ciprofloxacin resistance rapidly declines in *nfxB* defective clinical strains of *Pseudomonas aeruginosa*, Nat. Commun. **16**, 4992 (2025).

[57] K. M. Pluchino, M. D. Hall, A. S. Goldsborough, R. Callaghan, and M. M. Gottesman, Collateral sensitivity as a strategy against cancer multidrug resistance, Drug Resist. Updat. **15**, 98 (2012).

[58] A. Dhawan, D. Nichol, F. Kinose, M. E. Abazeed, A. Marusyk, E. B. Haura, and J. G. Scott, Collateral sensitivity networks reveal evolutionary instability and novel treatment strategies in ALK mutated non-small cell lung cancer, Sci. Rep. **7**, 1232 (2017).

[59] B. Zhao, J. C. Sedlak, R. Srinivas, P. Creixell, J. R. Pritchard, B. Tidor, D. A. Lauffenburger, and M. T. Hemann, Exploiting temporal collateral sensitivity in tumor clonal evolution, Cell **165**, 234 (2016).

[60] R. Loria, P. Vici, F. S. Di Lisa, S. Soddu, M. Maugeri-Saccà, and G. Bon, Cross-resistance among sequential cancer therapeutics: An emerging issue, Front. Oncol. **12**, 877380 (2022).

[61] N. Danisik, K. C. Yilmaz, and A. Acar, Identification of collateral sensitivity and evolutionary landscape of chemotherapy-induced drug resistance using cellular barcoding technology, Front. Pharmacol. **14**, 1178489 (2023).

[62] R. A. Gatenby, A. S. Silva, R. J. Gillies, and B. R. Frieden, Adaptive therapy, Cancer Res. **69**, 4894 (2009).

[63] J. West, L. You, J. Zhang, R. A. Gatenby, J. S. Brown, P. K. Newton, and A. R. A. Anderson, Towards multidrug adaptive therapy, Cancer Res. **80**, 1578 (2020).

[64] E. Rojo-Molinero, M. D. Macià, R. Rubio, B. Moyà, G. Cabot, C. López-Causapé, J. L. Pérez, R. Cantón, and A. Oliver, Sequential treatment of biofilms with aztreonam and tobramycin is a novel strategy for combating *Pseudomonas aeruginosa* chronic respiratory infections, Antimicrob. Agents Chemother. **60**, 2912 (2016).

[65] M. Müsken, V. Pawar, T. Schwebs, H. Bähre, S. Felgner, S. Weiss, and S. Häussler, Breaking the vicious cycle of antibiotic killing and regrowth of biofilm-residing *Pseudomonas aeruginosa*, Antimicrob. Agents Chemother. **62**, e01635-18 (2018).

[66] J. Molina-Hernández, Optimization of sequential therapies to maximize extinction of resistant bacteria through collateral sensitivity, Zenodo (2026), 10.5281/zenodo.18656444.